UNIVERSITY OF CALIFORNIA

Santa Barbara

Tumbling Stacks of Purine Crystals Create Sparkling Iridocytes in the Nudibranch, *Flabellina iodinea*

A Thesis submitted in partial satisfaction of the
requirements for the degree Master of Arts
in Molecular, Cellular and Developmental Biology

by

Savannah Jane Dearden

Committee in charge:

Professor Daniel E. Morse, Chair

Professor Kathleen R. Foltz

Professor Todd H. Oakley

June 2016

The thesis of Savannah Jane Dearden is approved.

_____
Kathleen R. Foltz

_____
Todd H. Oakley

_____
Daniel E. Morse, Committee Chair

June 2016

Tumbling Stacks of Purine Crystals Create Sparkling Iridocytes

in the Nudibranch, *Flabellina iodinea*

by

Savannah Jane Dearden

ACKNOWLEDGEMENTS

This work is dedicated to my mother, Kimberly Dearden, who taught me that much of the beauty in this world lies underwater.

I would also like to sincerely thank Daniel E. Morse, Amitabh Ghoshal, Mary Baum and Daniel DeMartini for their many hours of instruction and mentorship, Geoffrey Lewis for his microscopy expertise, Stephan Kraemer for assistance with electron diffraction, Jerome Santos for his daily enthusiastic support, Kori Lay for the embedding protocol and the nudibranchs of Goleta Pier for both their beautiful morphology that both enabled and inspired this work.

ABSTRACT

Tumbling Stacks of Purine Crystals Create Sparkling Iridocytes

in the Nudibranch, *Flabellina iodinea*

by

Savannah Jane Dearden

Although pigments contribute much of the brilliant purple and orange coloration of the aeolid nudibranch, *Flabellina iodinea,* the brightness of both colors was found to be enhanced by unusually sparkling iridocytes that exhibit rapid temporal variation in the brightness of their reflectivity. Electron micrographic examination revealed these epidermal cells to contain numerous multilayer stacks of crystals, both within vesicles and apparently free in the cells. High-resolution light microscopy showed that these structures tumble freely to produce the observed sparkling reflectivity. Most abundant near the epithelial basal lamina, the perceived color of these sparking iridocytes appears dependent on the size and thickness of the crystal platelets that comprise the stacks, with those that exhibit silver reflectance in the orange cerata being larger and thicker than those that reflect blue in the epithelium of the purple body. Thin layer chromatography and UV spectrometry show that the crystals isolated from all epithelial regions are identical in composition, with guanine as the major component and its derivative, hypoxanthine, a minor component. Electron diffraction of the crystals isolated from the orange and purple tissue exhibit nearly identical lattice parameters of $a = 6.57 \pm 0.05$ Å, $b = 13.65 \pm 0.07$ Å and $c = 18.76 \pm 0.06$ Å - unit cell

dimensions that closely match those measured for the non-tumbling guanine crystals widely distributed in other biophotonic systems ranging from marine invertebrates to terrestrial vertebrates. The epidermal iridocytes of *F. iodinea* are thus capable of manipulating crystal growth to produce multilayer stacks of purine crystals with optical properties specific to different locations in the body. This specificity parallels and apparently augments the animal's striking pattern of pigmentation.

TABLE OF CONTENTS

LIST OF FIGURES

I. INTRODUCTION

Lacking shells, the marine nudibranch molluscs *(Opisthobranchia: Gastropoda)* have evolved a diversity of alternate defense mechanisms, including chemical secretions and sequestration of stinging nematocysts from their prey, with concomitant patterns of bright coloration recognized as warning by potential predators (Thompson, 1960b; Edmunds, 1966; McBeth, 1972; Martin, 2003; Aguado and Marin, 2007). *Flabellina iodinea* (Cooper, 1863), an aeolid nudibranch native to the west coast of North and Central America, exhibits a color pattern that is striking, even amongst other marine opistobranchs (Figure 1). The body is purple-blue while its dorsal cerata (facilitating digestion and gas exchange) are brilliant orange. This beautiful morphology, coupled with its rhythmic flexions propelling it through the water (Goodheart, 2013), have earned this species the nickname "the "Spanish shawl." Feeding preferentially on the cnidarian hydroid *Eudendrium ramosum* (McBeth, 1972), *F. iodinea* sequesters the prey's stinging nematocysts, storing them in the tips of the cerata in specialized structures known as cnidosacs (Martin, 2003; Greenwood, 2009; Martin, 2009). It has been proposed that this color pattern, in which the brightly colored cerata contrast sharply with the body, may additionally function to attract predators to the location of the stinging nematocysts and away from the visceral organs. The ability of the aeolids to autotomize and regenerate their cerata supports this hypothesis (Thompson, 1960a; Edmunds, 1966; Miller, 2000; Fleming, 2007), as does the observation that when attacked, aeolids typically contract the body and the rhinophores, while holding the cerata more erect and oriented towards the attacking predator (Edmunds, 1966; Aguado and Marin, 2007).

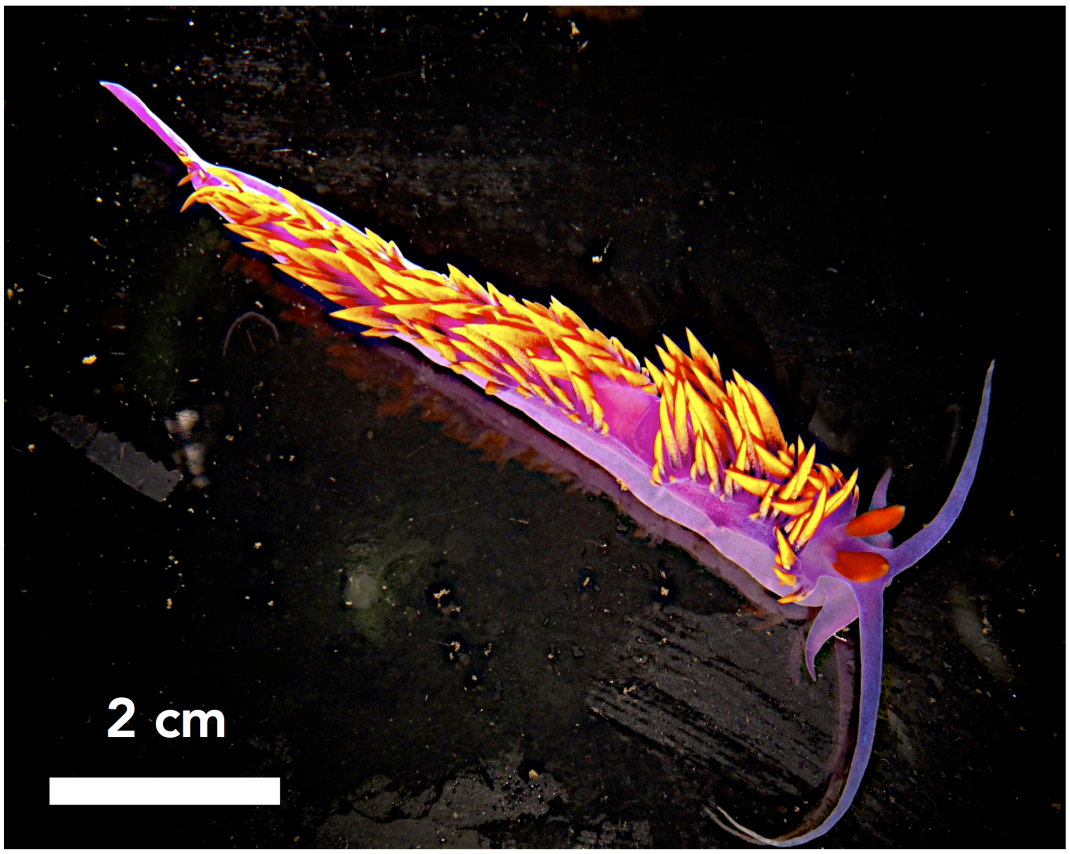

Figure 1. Live *F. iodinea*, illustrating contrast between bright orange cerata and purple body.

The bright orange, purple and red seen in Figure 1 are produced by the carotenoid pigment, astaxanthin, and its esters, that are concentrated in granules in the epidermal cells (McBeth, 1972). We have found that these pigments alone, however, do not account for the brilliant colors of the tissues of *F. iodinea* in their entirety. Intermingled with the pigmented colors, we discovered highly reflective regions of the tissue as shown in Figure 2.

Similar reflective regions have been observed in the epidermal tissues of other nudibranchs. Burgin described vacuoles filled with small particles of a "striking metallic luster" seen "only in reflected light" in the aeolid *Hermissinda crassicornis* (Eschscholtz, 1831), and noted similar structures in a number of other aeolid species (Burgin, 1964). Similarly, in *Flabellina affinis* (Gmelin, 1791), a congener of the species studied here,

Martin et al. described “pigment inclusions” filled with “iridescent platelets” near the nuclei of certain epidermal cells (Martin and Walther, 2002; Martin et al., 2007).

Reflective structures have arisen many times through the course of evolution in very distantly related species, but are particularly prevalent in the tissues of marine animals, where they are tailored to the limited light environment in which these organisms live (Denton, 1970). High reflectivity in biological tissues - a result of “structural color” fundamentally different from the differential absorption and reflectance by pigments - is most often the result of thin-film interference. The structures responsible, described as multilayer reflectors, are composed of stacks of materials of alternating high and low refractive index, with reflection occurring from each of the successive interfaces (Vukusic and Sambles, 2003). Total reflectance increases proportionally with the difference in refractive indices of the alternating layers and with the number of layers in a stack (Land, 1972). The reflected light may be either silvery or white (i.e., broadband, comprised of multiple wavelengths) or a specific color, depending on the relative constancy or variability of spacing, and the dimensions and refractive indices of the layers (Land, 1972). In both marine and terrestrial animals, the high refractive index layers have been found to be comprised of a wide range of materials including collagen (Denton, 1970) and other condensed proteins (Crookes et al., 2004; DeMartini et al., 2013), chitin (Denton, 1970; Seago et al., 2009) and crystals of guanine (Levy-Lior et al., 2010a; Dougherty et al., 2014; Hirsch et al., 2015; Gur et al., 2015; Teyssier et al., 2015). The low refractive index layer is most often cytoplasm (Jordan et al., 2014).

We describe here the uniquely sparkling (temporally varying) reflective structures discovered in epidermal iridocytes of the nudibranch, *Flabellina iodinea.* Sparkling reflectivity originates from freely tumbling, multilayer stacks of platelets composed of

purine crystals both contained in intracellular vesicles and apparently free in the cytoplasm. Identified *in situ* by light microscopy and TEM, the platelets were isolated from the tissue, characterized by electron diffraction, and their composition analyzed by thin-layer chromatography and UV spectroscopy. The reflective structures are composed primarily of guanine and traces of the related hypoxanthine, arranged in stacks of thin, flat crystals, each approximately 200-800 nm across the widest face and 50-200 nm thick.

II. MATERIALS AND METHODS

A. Specimens

Flabellina iodinea nudibranchs were collected at a depth of ca. 4 m from Goleta Bay, CA (34 24.854'N 119 49.711'W). The animals were kept in fresh flowing seawater with their hydroid food, *E. ramosum*, for 1-60 days before study.

B. Light Microscopy of Live Tissues

Light microscopy was used to analyze the epidermis of whole live specimens (in glass petri dishes) and small pieces of cerata and main body tissue (on glass slides under cover slips), all in artificial seawater (ASW = (70 mM NaCl, 10 mM KCl, 27 mM $MgCl_2$, 29 mM $MgSO_4$, 11 mM $CaCl_2$, 10 mM HEPES, pH 7.8) (Kester et al., 1967). Observations were performed on a Zeiss AxioObserver D1M inverted microscope (Carl Zeiss AG, Oberkochen, Germany). The samples were imaged in both transmission and reflection mode, with illumination from a broadband halogen lamp (with detectible light in the range of 200-800 nm) and Zeiss EC EpiPlan-NEO-FLUAR objectives. Intensity analysis and particle tracking were performed with series of images in ImageJ software (Schneider et al., 2012).

C. Fixation, Light Microscopy and TEM

Specimens were euthanized by decapitation. Entire cerata and segments of main body tissue were excised and chemically fixed in utrafilter-sterilized ASW containing 2% formaldehyde plus 2% glutaraldehyde for 2 h at room temperature. The tissue was then

washed in ASW twice for 30 min each and post fixed in 2% osmium tetroxide for 1 h at room temperature. The fixed tissue was then dehydrated in a series of graded ethanol solutions: 25, 50, 75, 90, 100, 100 and 100 (% ethanol in degassed, deionized water); this was followed by solvent exchange into propylene oxide/ethanol solutions: 33, 66, 100 and 100 (% propylene oxide). The tissue was then transferred to EMbed 812 embedding media (EMS, catalog # 14120) through a gradient series of resin/propylene oxide solutions: 33, 66, 100 and 100 (% EMbed 812 resin), then transferred to silicone molds, overlaid with fresh resin and cured overnight at 55 °C. The hardened blocks were trimmed and sectioned to 500 nm (light microscopy) or 100nm (electron microscopy) slices on a Leica EM UC6 ultramicrotome (Leica Microsystems, Wetzlar, Germany). 500 nm sections were transferred to glass slides (Fisher Scientific, catalog # 413051) and stained with 25% methylene blue, 25% azure B, 25% toluidine blue, 10% sodium borate for 45- 60 s. Excess moisture was wicked away and the samples were mounted beneath a glass coverslip (Fisher Scientific, catalog # 413521) with Permount™ (Fisher Scientific, catalog # 17986). 100 nm sections were transferred to copper/Formvar grids (Ted Pella, Substratek™, 75 Square Mesh, #1802-F). Post-stain procedures for 100 nm sections observed with electron microscopy varied, with the sample being treated either with (A) 2% aqueous uranyl acetate (15 min) and 0.5% aqueous lead citrate (1 min) with 3X20 s DI H_2O washes in between; (B) only 2% aqueous uranyl acetate (15 min); or (C) only 0.5% aqueous lead citrate (1 min); each of these procedures was followed by 3 washes of 20 s with distilled H_2O. All grids were air dried after post-staining.

All light microscopy observations of 500 nm sections were performed with a Zeiss AxioObserver D1M inverted microscope (Carl Zeiss AG, Oberkochen, Germany) as used

for the live tissues. 100 nm sections were viewed with a JEOL 1230 Transmission Electron Microscope (TEM) operating at 80 kV.

D. Purification and TEM of Platelets

Purification of the electron dense platelets observed in the tissue sections was achieved through adaptation of the protocol of Levy-Lior et al. for purification of guanine crystals from spider integument (Levy-Lior et al., 2010a). Live *F. iodinea* were rinsed gently in ASW, then euthanized by decapitation. The orange cerata and bright regions of the purple main body were removed and separately digested with Proteinase K (Roche, catalog # 311587001) in DI water at a concentration of ~3.46 U/mL for 3 d at room temperature with shaking. The samples were vortexed for 30s every 24 h. Samples were centrifuged at 11,934 xG (10600 rpm, Eppendorf 5810 R) for 20 min at room temperature. The pellets were washed with DI water by centrifugation and tissue and cell debris were removed with the supernatants. The pellets were resuspended in DI water and the same centrifugation process was repeated multiple times until the supernatants were clear and the pellets a solid white. The pellets were stored in DI water at 4^{o} C.

For examination by TEM, 2-5 μL of the suspensions of the pellets were deposited on copper/Formvar grids (Ted Pella, Substratek™, 75 Square Mesh, catalog # 1802). Crystals in the micro-droplet were allowed to settle for 1 min before excess moisture was wicked off. The grids were air dried and examined by TEM as described for above.

E. Electron Diffraction

Samples of the purified crystals prepared for examination by TEM as described immediately above also were analyzed by electron diffraction using a FEI Technai G2 Sphera transmission electron microscope operating at 200 kV after calibration with a gold standard. All diffraction patterns were acquired at a working distance of 520 mm without tilting the stage.

F. UV-Vis Spectroscopy

Standards of pure guanine (Sigma Aldrich, catalog # G11950) and hypoxanthine (Sigma Aldrich, catalog # H9377) (between 0.01 mM to 0.10 mM) were dissolved in the TLC solvent (see below) and samples of the purified biogenic crystals dissolved in the same solvent and clarified by centrifugation at 20,817 xG (14,000 rpm, Eppendorf 5810 R) for 5 min at room temperature were analyzed for absorbance in the range of 200-400 nm using a Jasco V-600 Ultra Violet-Visible (UV-Vis) spectrophotometer and a 10 mm path-length quartz cuvette (Hellma®, Sigma Aldrich, catalog # Z803669) with the TLC solvent used as a blank reference. Molar extinction coefficients for the guanine and hypoxanthine standards were determined at their respective wavelengths of maximal absorbance, enabling estimation of the approximate concentrations in the biogenic samples.

G. Thin Layer Chromatography

Analysis by thin layer chromatography (TLC) was conducted using the method of Rohrlich and Rubin (1975). The purified and washed platelets from *F. iodinea* cerata and

body tissue were pelleted by centrifugation, dissolved in a small volume of 1.0 N HCl and analyzed on glass-backed microgranular cellulose chromatograms in parallel with authentic guanine (Sigma Aldrich, catalog # G11950) and hypoxanthine (Sigma Aldrich, catalog # H9377) applied in the same solvent. All samples were clarified by centrifugation at 20.817 xG (14,000 rpm, Eppendorf 5810 R) for 5 min at room temperature prior to chromatography. Chromatograms were developed with a methanol-HCl-water (70:20:10 v/v/v) solvent for ~45 min and visualized with short wave UV light.

III. RESULTS

A. Light Microscopy of Living Tissue

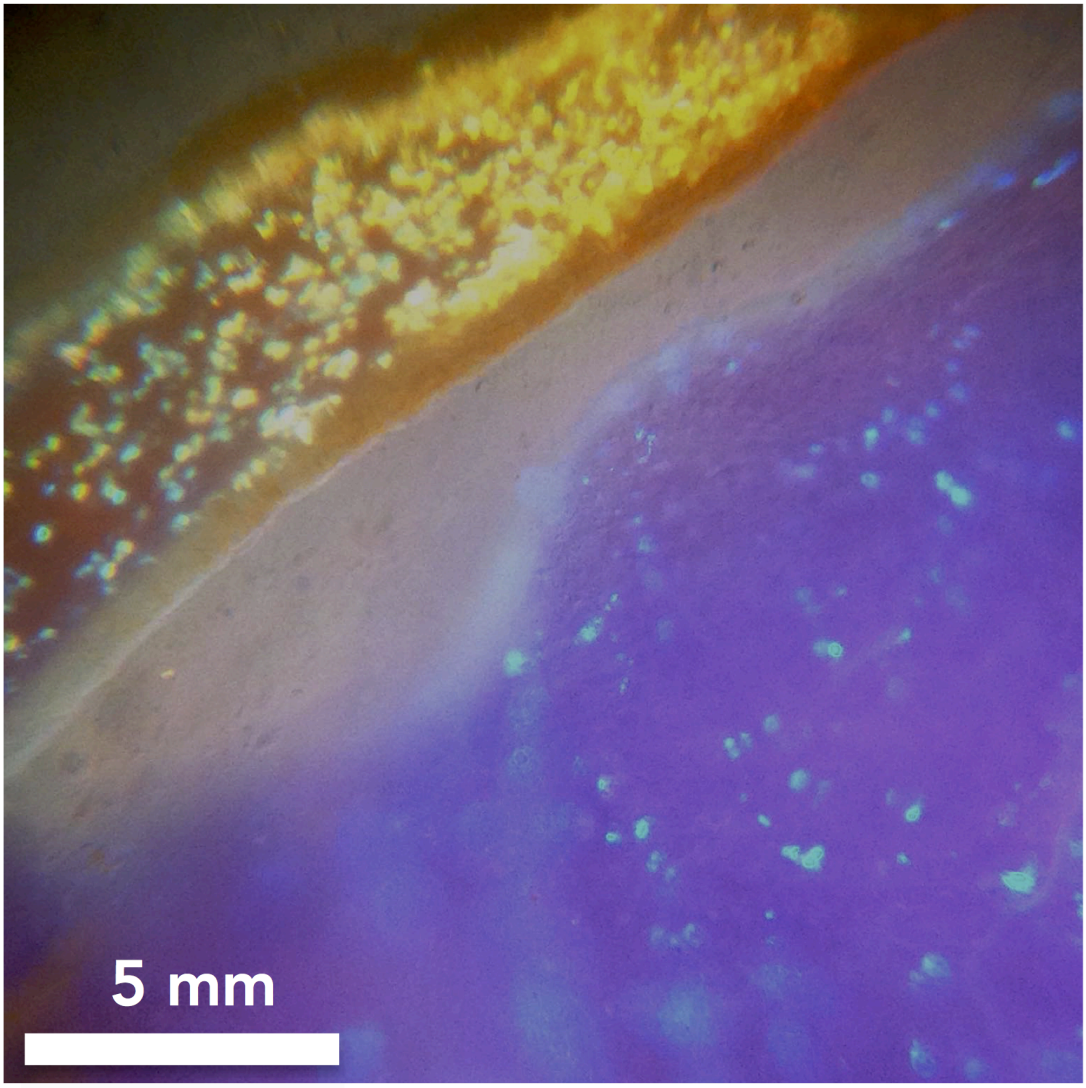

Figure 2. Magnified view of the epidermis of a live *F. iodinea*, revealing regions of bright reflectivity in the orange cerata and purple body; note the higher density of the reflective regions in the cerata relative to the body.

The dermis of the aeolid nudibranch, *Flabellina iodinea*, is speckled with spherical regions 5 to 10 μm in diameter filled with dynamically reflecting structures. Figure 2 illustrates the brilliance of these reflective regions in a live, whole specimen under

illumination. These regions, while present across all areas of the main body and cerata examined, are most abundant in the orange cerata (Figure 2). The appearances of these regions in the cerata and the main body are compared in the series of light micrographs shown in Figure 3. These micrographs of small samples of excised live tissues under cover slips in ASW demonstrate the differences in relative abundance and color of the reflective regions in the cerata and main body. While these regions appear dark brown in the cerata and lighter brown in the main body when observed in bright field transmission mode, these same regions viewed in reflectance mode appear bright silver and blue in the cerata and main body respectively.

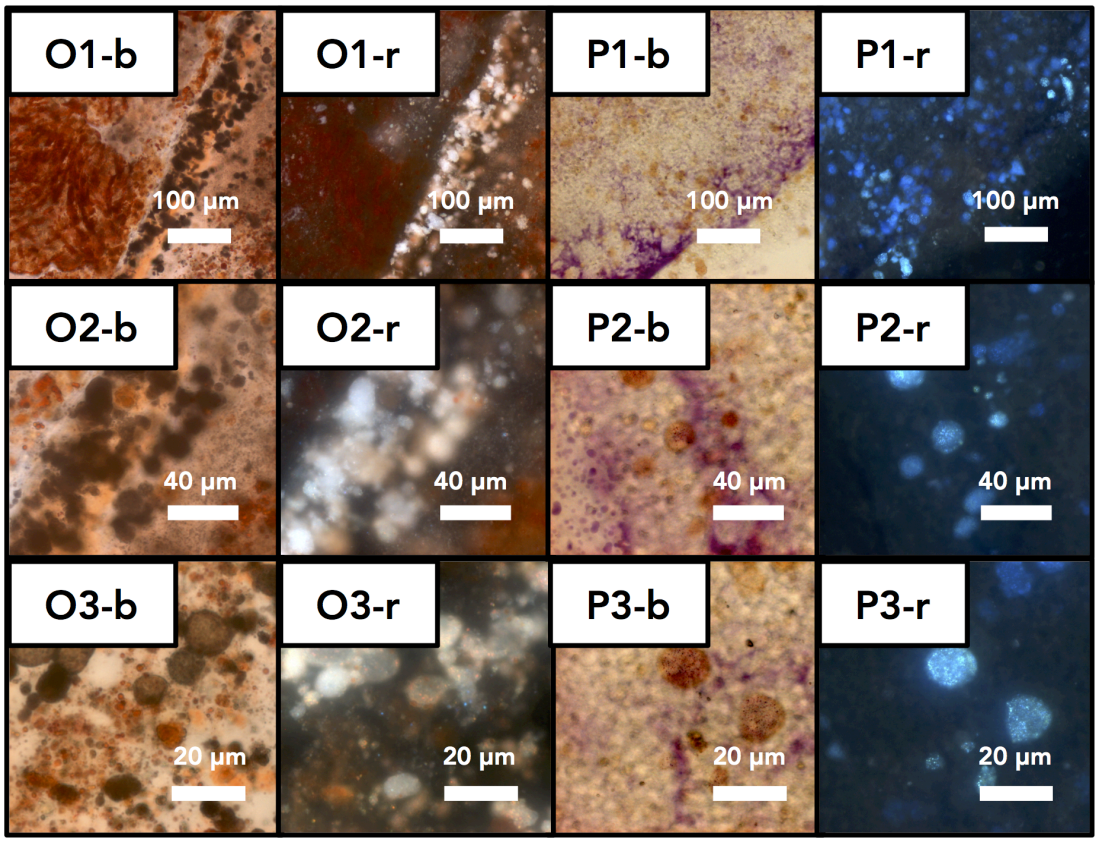

Figure 3. Light micrographs of live *F. iodinea* tissues from orange cerata (O) and purple foot (P) viewed in ASW with bright field transmission ("b") or dark field reflection mode ("r") at progressively increasing magnification (1-3).

Higher magnification reveals that these regions are composed of punctate reflecting structures less than a micron in size (visible in Figure 3- O3-r and P3-r). While the majority of the punctate reflectors are contained in the regions described, many also were observed free in the surrounding tissue and medium.

The punctate reflective structures are not stationary, but, instead, move rapidly and without any determined pattern, as might be expected for small particles in Brownian motion. This motion is readily evidenced in the intermittent reflectance of light from these structures, giving rise to their pronounced, temporally sparkling appearance – the tracking of which is shown in Figure 4. This effect was not distinctly related to the reflectors' compartmentalization to the described regions. While free reflectors did exhibit a greater range of intensity values, this is attributable to decreased background intensity from surrounding reflectors compared to those concentrated in compartments (Figure 4- B and C). Some membrane bound compartments appear more densely packed with reflective particles than others; the movement of the particles within these more crowded compartments was observed to be reduced relative to that of the free reflectors. These dynamic movements, illustrated in the epidermal tissue from the ceras in Figure 4, are found ubiquitously across all areas of reflective tissue.

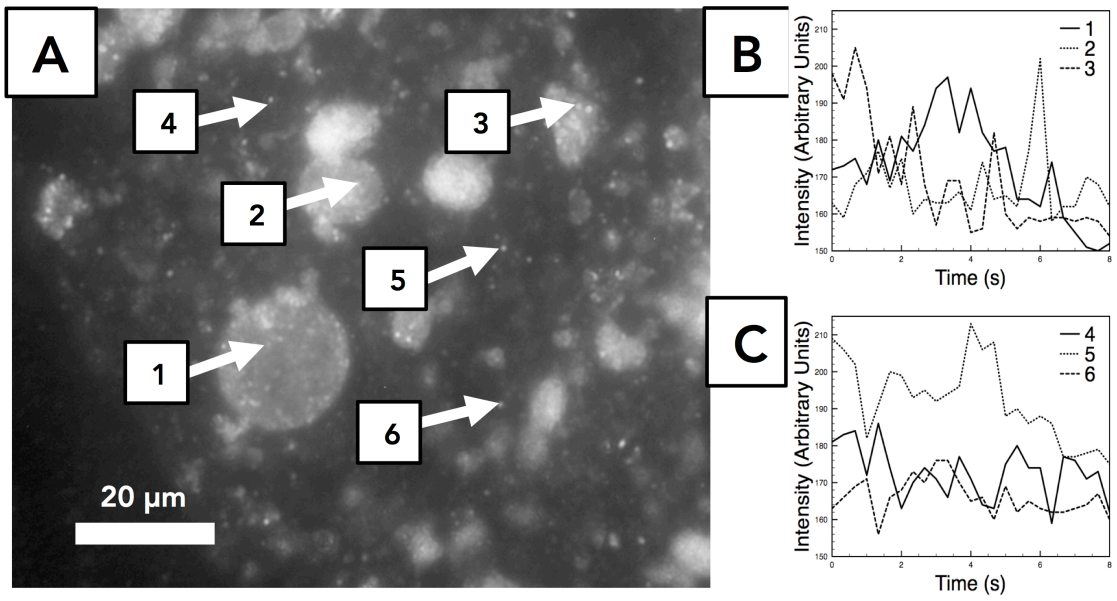

Figure 4. Temporal tracking of reflectivity suggesting Brownian motion. (A) Light micrograph of live *F. iodinea* tissue observed in dark field reflection mode. Examples of compartmentalized reflective sources are marked by arrows 1, 2, and 3; un-compartmentalized sources by arrows 4, 5 and 6. Intensities of reflectivity from these single sources were tracked over time using ImageJ as described in Methods. Graphical representations of the temporal variation of intensity of reflectance from the selected compartmentalized (B) and un-compartmentalized (C) sources are shown at right.

B. Examination of Fixed Tissues by Light Microscopy and TEM

Light microscopy of the 500 nm thick sections of the fixed and embedded tissue stained with methylene blue, azure B and toluidine blue verified that the epidermal ultrastructure of *F. iodinea* is similar to that of other aeolids (Martin and Walther, 2002; Martin et al., 2007), with only a single cellular layer of polarized epidermal cells between the well defined basal lamina and the protective external layer of mucus. Cross sections of a single ceras (Figure 5) show the endothelial monolayer (EM) delineated from the more interior muscular tissues and core digestive diverticulum (DD) by the basal lamina (BL). Many darkly staining secretory glands (SG) in the endothelial monolayer are also visible. The reflective structures were not visible in this preparation.

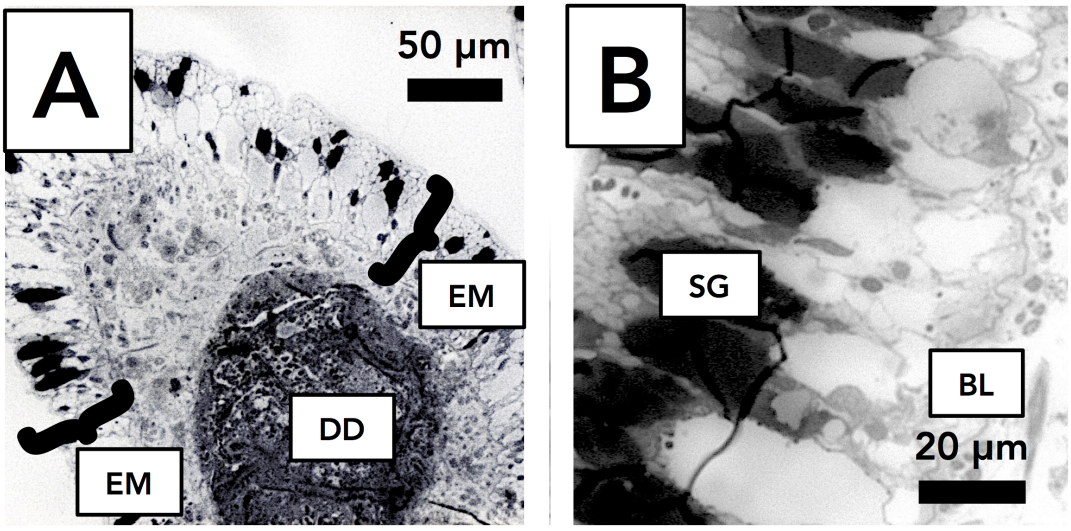

Figure 5. *F. iodinea* tissues viewed by light microscopy after fixation and staining with methylene blue-azure B- toluidine blue as described in Methods. (A) Isolated ceras showing epithelial monolayer (EM) delineated from the inner muscle and digestive diverticulum (DD). (B) Cells of the epithelial monolayer, with darkly stained secretory glands (SG) and basal lamina (BL) at the base of the epithelial cells clearly visible.

TEM of 100 nm thin sections stained after fixation with uranyl acetate and lead citrate (Figure 6) revealed numerous membrane-bounded envelopes, some of which appeared as empty voids, approximately 500 nm across and 100-200 nm in height, near the basal lamina, where reflective pigment granules have been described in other nudibranch species (Burgin, 1964; Martin and Walther, 2002;Martin et al., 2007). Electron dense, stacks of two to eight plate-like deposits of material are present both within and in close proximity to these envelopes. The individual platelets in these fully stained sections vary in size between 300 and 600 nm across the flat face and 100-200 nm in thickness parallel to the stacking direction. Each platelet within a stack is separated from the next by a thin layer of lightly stained material (Figure 6-1). The apparently empty voids are of the corresponding size, shape and spacing to have been left by dissolution of the material in the dense platelets.

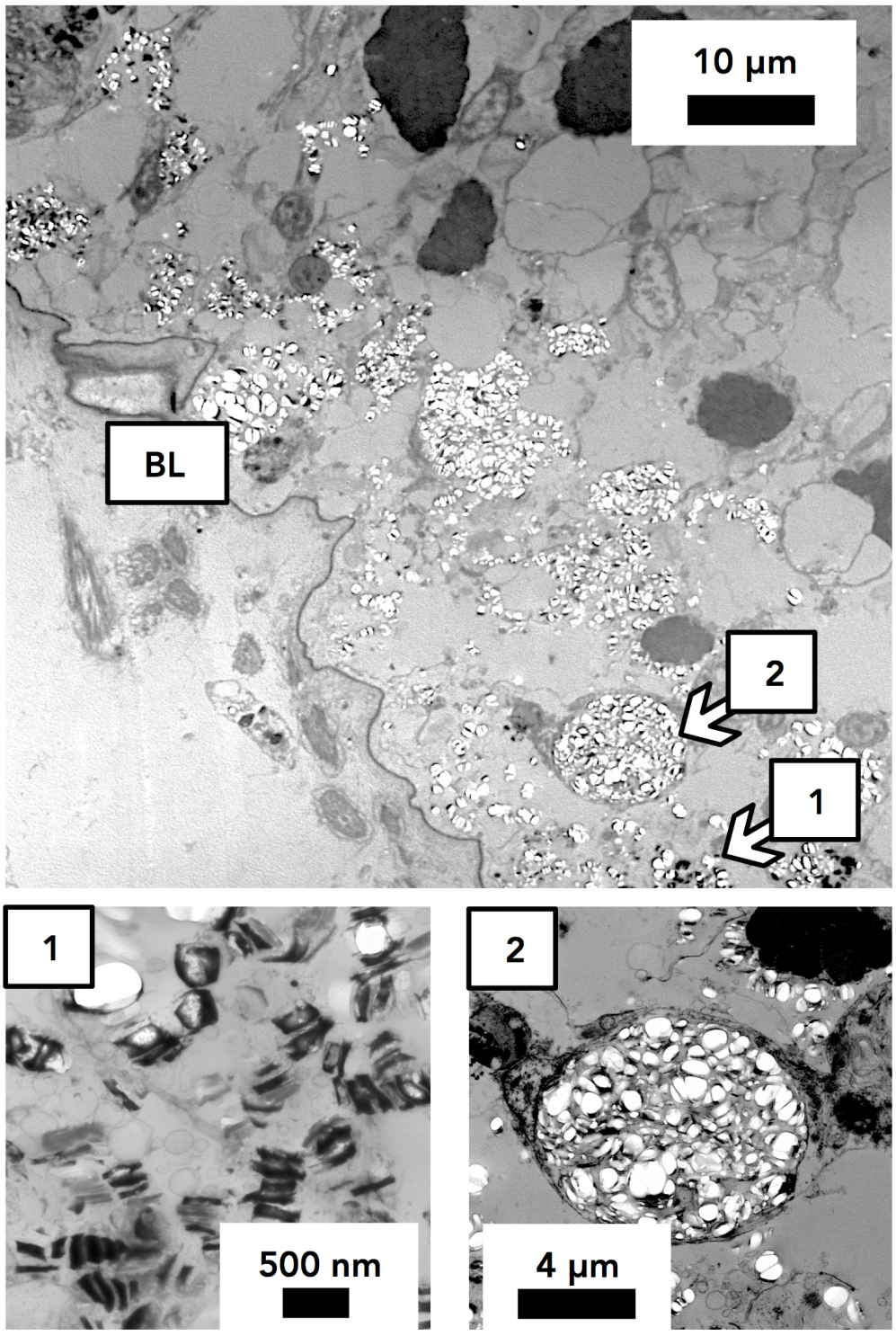

Figure 6. TEM reveals numerous stacks of electron dense platelets near the epithelial basal lamina of *F. iodinea* cerata. Tissue from the epithelial monolayer stained with lead citrate and uranyl acetate; arrows 1 and 2 indicate regions of interest magnified in panels 1 and 2. Note conspicuous white voids remaining after apparent dissolution of electron-dense platelets visible "free" within the cells (1) and compartmentalized within membrane bound structures (2).

To determine whether the post-fixation staining with lead citrate was responsible for dissolution of the electron dense platelets, as had previously been reported for purine-based crystals (Land, 1966; Schmitter, 1971; Levy-Lior et al., 2010b; Mueller and Labhart, 2010), fixed sections were treated with only lead citrate, only uranyl acetate, both compounds or neither. Samples treated with lead citrate (alone or in combination) exhibited the apparently empty voids while those that were either not stained or treated only with uranyl acetate did not exhibit any voids and, in their place had more platelet-containing envelopes (Figure 7). This indicates that the platelets are composed of materials, very likely purines, soluble in lead citrate.

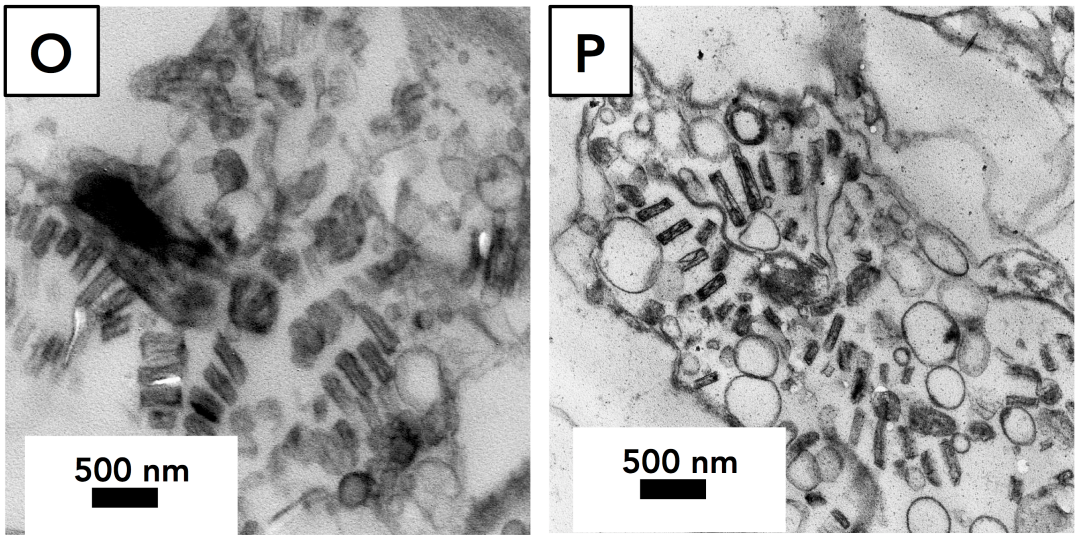

Figure 7. Stacks of electron dense platelets are present in all regions of the epithelium that are visibly reflective. Cross sections (100 nm) of cells in the epithelial monolayer from either the cerata (O) or the body (P), stained with uranyl acetate, illustrating the presence of stacks of electron dense platelets in both parts of the body, but with varied dimensions.

While visible in the cells of the epithelial monolayer near the basal lamina in both the cerata and the main body, the platelets were much more common in the cerata. In both areas of tissue sectioned, platelet-containing envelopes or voids were found concentrated in

intracellular membrane-bound compartments (Figure 6-2) as well as dispersed within the tissues (Figure 6-1), as also observed in light microscopy (Figure 3 and Figure 4). In samples stained with only uranyl acetate, the platelets in sectioned cerata ranged in width from 150-500 nm and 80-150 nm in height with 50-150 nm of space separating each platelet (Figure 7-A). In comparable sections of the main body stained with uranyl acetate, the platelets ranged in width from 200-500 nm and 80-100 nm in height with 100-130 nm of space in between them (Figure 7-B). Generally, space between each platelet is more readily visible in sections from which the lead citrate stain was omitted (Figure 7) compared to sections stained with lead citrate and uranyl acetate (Figure 6).

C. Purification and TEM of Crystals

The end product of the purification procedure [adapted from Levy-Lior et al.'s (2010) process for purifying crystals from spider integument] was a pellet of white material. Suspension of this material in DI water produced a cloudy white suspension that clarified over time. Tissue from the cerata and the main body of the nudibranch were processed separately; notably less material was recovered from the main body than from the cerata, when starting with the same tissue mass. The contents of the pellets were examined by depositing 3-5 μL of the initial suspension onto carbon coated TEM grids that were then air dried before imaging. The preparations consistently covered the TEM grids with electron dense, angular platelets and little to no cell debris visible (Figure 8). The platelets are apparently crystalline and heterogeneous in size or shape. The smallest have a face of 180 nm across and the largest at 800 nm across with some exhibiting a prismatic habit and others a hexagonal one. Figure 8 shows a typical overview electron micrograph of one of these

preparations. The size, shape and yield of the crystals strongly suggest that they are the same platelets that were identified in the *in situ* micrographs.

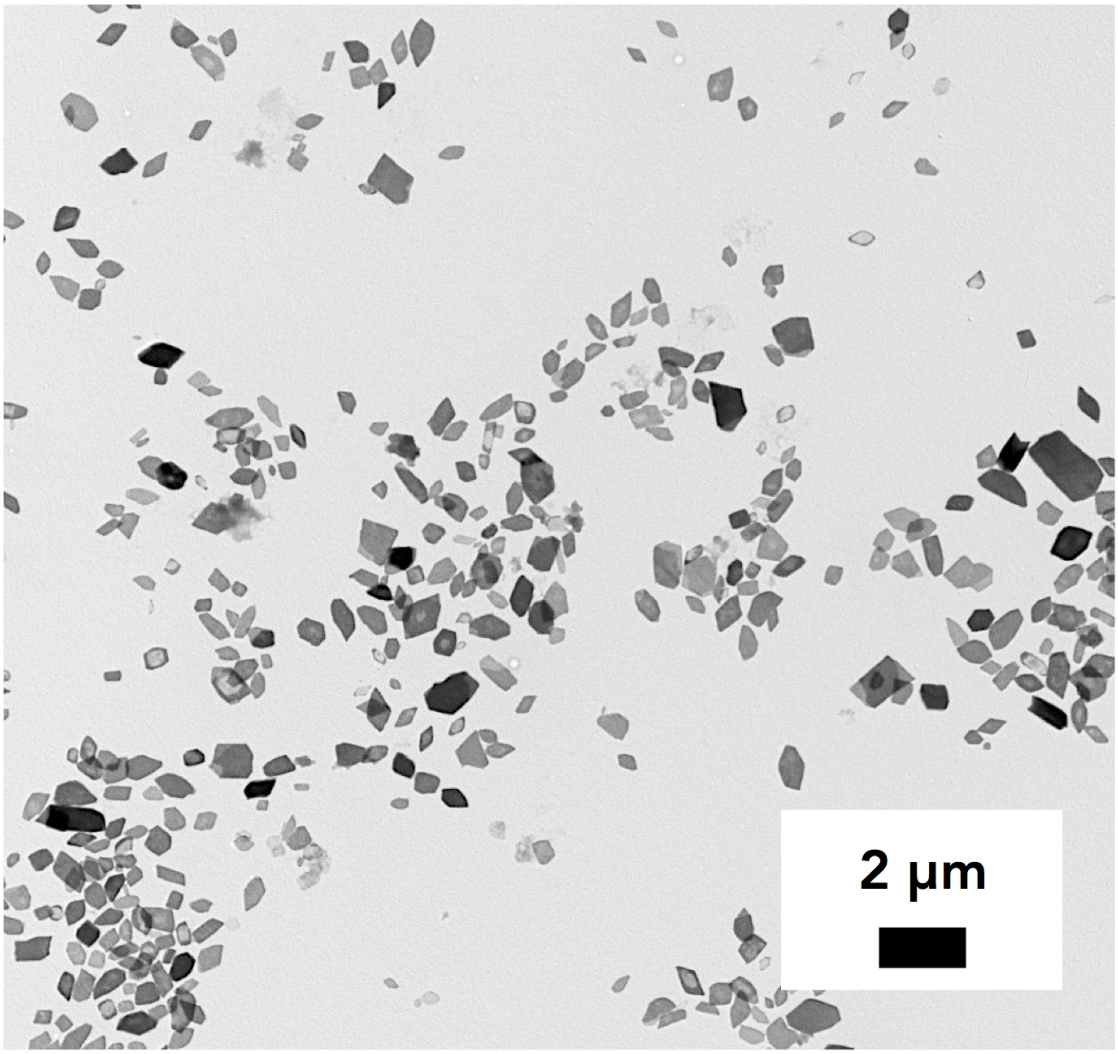

Figure 8. An array of purified crystals from cerata and body. TEM of the angular, electron dense platelets constituting the major component of the pellet obtained from the purification procedure. Note that the platelets correspond in size to those viewed *in situ* (*cf.* Figures 6 and 7).

The mean values of crystal dimensions ± the standard deviation were determined. The platelets isolated from the cerata are larger (590 ± 50 nm; n = 50) measured through their longest dimension than those isolated from the body (320 ± 35 nm; n = 50) measured

through their longest dimension and appear denser or thicker (darker) in the electron micrographs (Figure 9).

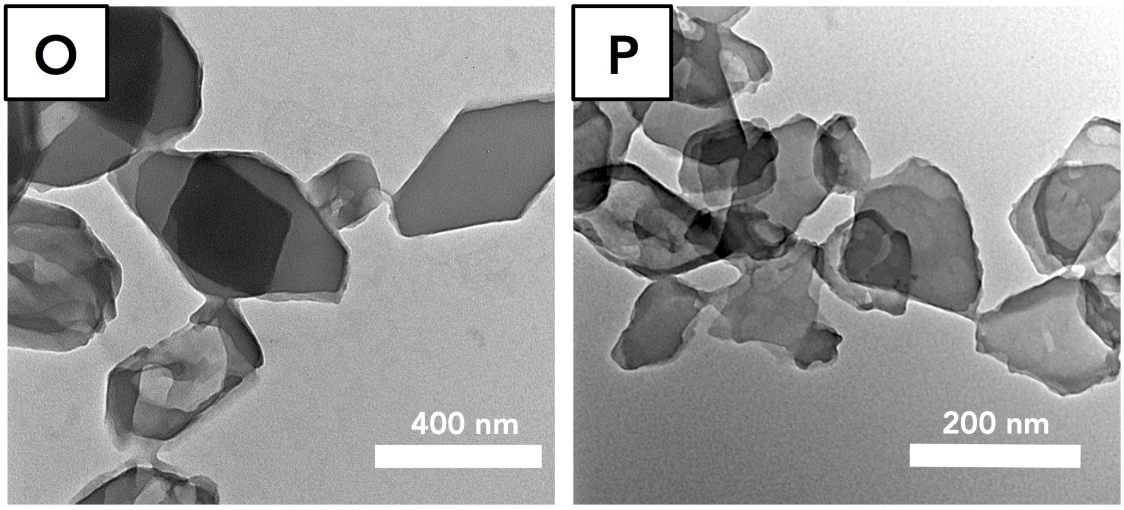

Figure 9. TEM micrographs of platelets purified from the orange cerata (O) and the purple body (P). Note larger size and greater electron density of crystals from the cerata.

The purified individual platelets typically deposited flat, with their largest face exposed to the electron beam. Stacks of platelets were also isolated and these deposited with the face of the platelets, which is also the stacking direction, perpendicular to the electron beam, as shown in Figure 10. Images in this orientation facilitated precise measurement of the thickness of the crystals in the platelet stacking dimension: platelets measured from the cerata are roughly 120 ± 30 nm (n = 18) thick and those measured from the body are roughly 60 ± 15 nm (n= 12) thick (Figure 10; Figure 11- O2, P2). These dimensions are considered to be more accurate than those taken from *in situ* sections of tissues that were subject to dehydration and heavy metal staining; however, the spacing between the platelets seen *in situ* (Figures 6 and 7) is no longer visible in the purified stacks (Figure 10; Figure 11- O2, P2). Consequently, a measurement of equal quality for the inter-platelet spacing within the stacks could not be determined from the purified platelets.

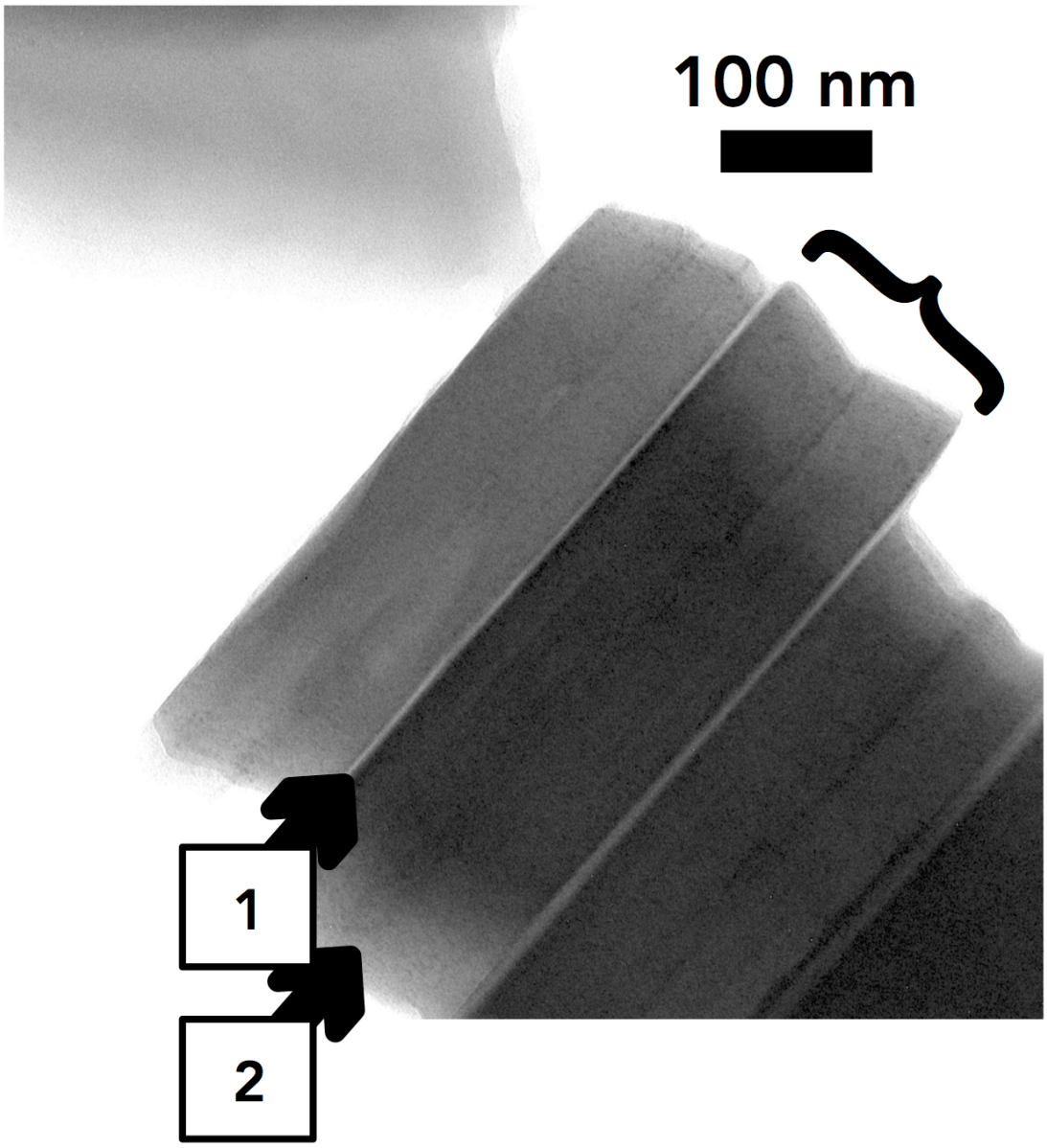

Figure 10. High magnification of a stack of crystals purified from the cerata illustrating how each dark, electron dense platelet, approximately 100 nm thick (denoted by the black bracket), is delineated from the next in the stack by a thin space (indicated by arrow 1) and composed of two tightly adherent layers (boundary between layers indicated by arrow 2).

The micrographs of purified platelets suggest that each individual platelet is composed of two layers. These layers are visible along the edges of crystals deposited flat, on their largest face (Figure 9; Figure 11, O1, P1), and in the edge-on view of the deposited the stacks of platelets (Figure 10, Figure 11, O2 and P2). Each sub-platelet layer is

approximately half the thickness of the platelet in which it is found. These sub-platelet layers appear to be composed of the same material with no evident space in between them.

D. Electron Diffraction

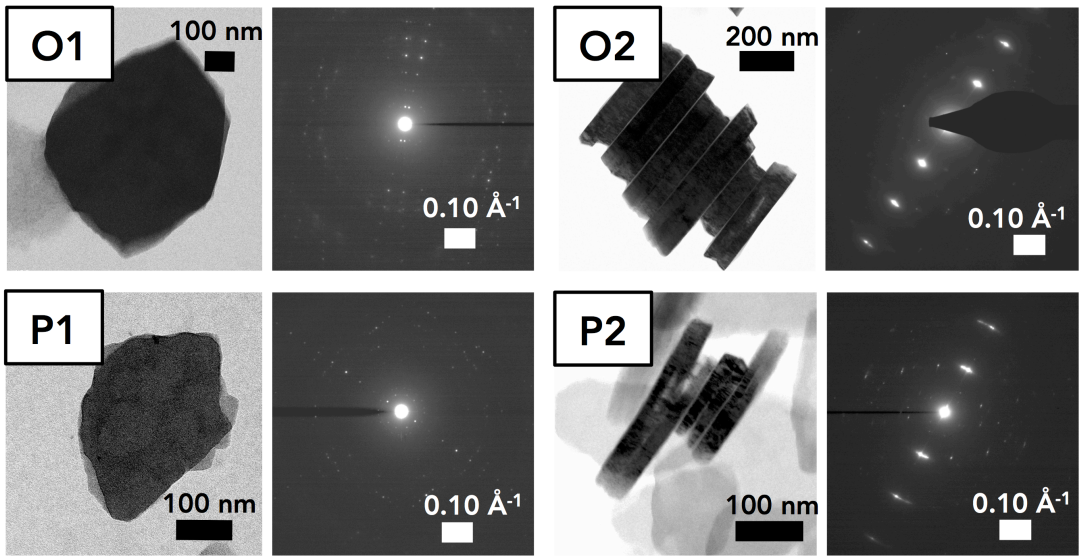

Figure 11. Transmission electron micrographs of purified platelets from the orange cerata (O1, O2) and the purple body (P1, P2) of *F. iodinea* and their corresponding electron diffraction patterns confirming crystallinity. O1 and P1 patterns were obtained with the beam perpendicular to the largest crystal face, providing two principal spacings (*b* and *c*). These patterns indicate the presence of two superimposed crystals, the edges of which are visible in the electron micrographs. O2 and P2 patterns were obtained with the beam perpendicular to the edge of a set of stacked crystals, providing an additional spacing (*a*). The lattice spacings determined from the ED patterns of crystals from the cerata and the body are nearly identical.

Electron diffraction (ED) patterns (Figure 11) confirm the crystalline nature of the purified platelets, and strongly suggest that they are composed of one or more purines, as determined for other electron-diffracting crystalline biophotonic structures from other species (Rohrlich and Rubin, 1975; Levy-Lior et al., 2010b; Gur et al., 2013; Hirsch et al., 2015). The deposition of *F. iodinea* crystals onto TEM grids along the flat face and stacked on their side permitted collection of diffraction patterns representing all three dimensions of

the crystal lattice, presented here as mean values ± standard deviation for n = 8 diffraction patterns. Two principal spacings were determined from patterns of individual crystal platelets laid flat on the grid (Figure 11- O1 and P1): 13.64 ± 0.02 Å and 18.77 ± 0.04 Å (purified from cerata) and 13.66 ± 0.05 Å and 18.76 ± 0.02 Å (purified from the body). Diffraction patterns taken from crystals stacked on their sides (Figure 11- O2 and P2) provided a single principle spacing of 6.60 ± 0.03 Å and 6.54 ± 0.02 Å (purified from the cerata and body, respectively).

The ED patterns obtained with the electron beam perpendicular to the largest face of a single platelet (Figure 11- O1, P1) generally indicate the presence of two superimposed crystals, slightly offset from one another. This crystallographic superposition is consistent with the TEM observation that each crystal platelet is a doublet of crystalline layers. The angle between these two layers, as measured from the diffraction patterns, is highly variable.

E. UV-Vis Spectroscopy

The purified crystals were dissolved in methanol-HCl-water (70:20:10 v/v/v) and analyzed for absorbance in the range of 200-400 nm. The dissolved species absorbed strongly in the UV, exhibiting an absorption spectrum characteristic of purine nucleobases with maximal absorbance, λ_{max}, at 249 ± 1 nm (Figure 12). Pure standards of guanine (λ_{max} = 249 ± 1 nm) and hypoxanthine (λ_{max} = 247 ± 1 nm) were analyzed in parallel. A near perfect fit of the *F. iodinea* absorbance spectrum was obtained with a spectrum simulated for a mixture of 81% guanine and 19% hypoxanthine (Figure 12-B).

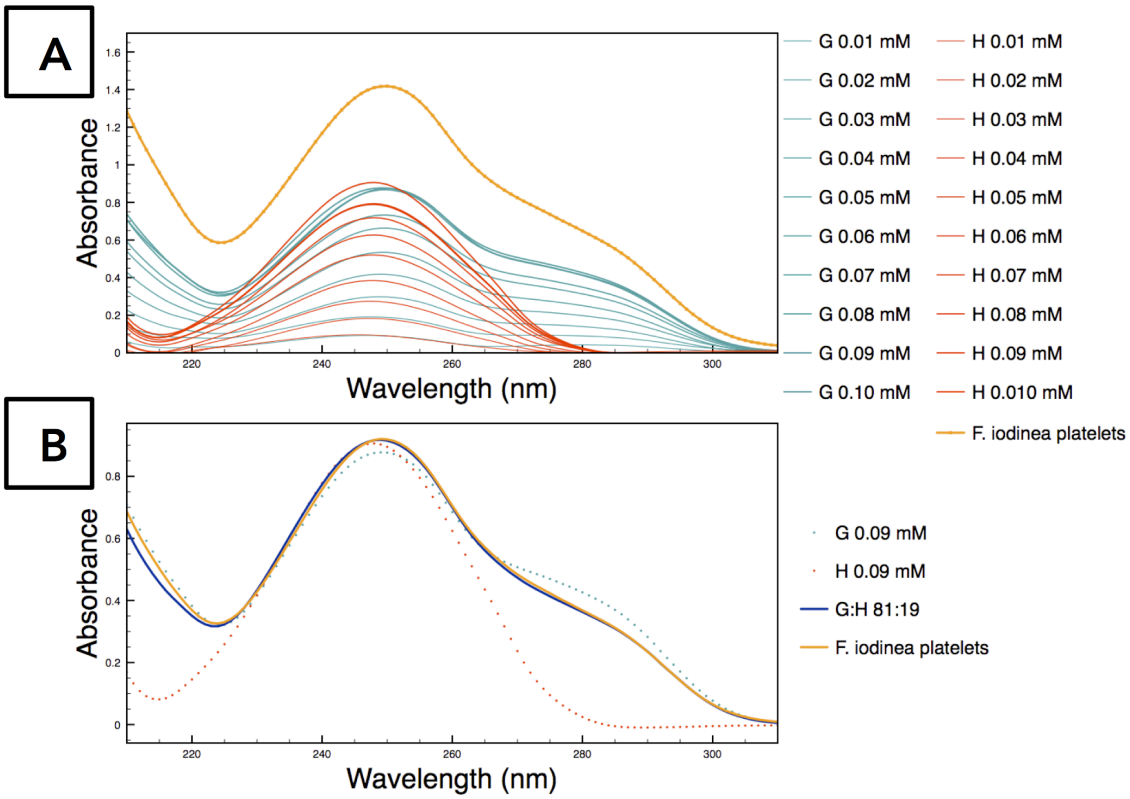

Figure 12. UV-Vis spectroscopy reveals that the purified crystals are comprised of purine. (A) Absorbance spectra of purified and dissolved crystals from *F. iodinea* cerata (orange) and pure guanine (teal) and hypoxanthine (red) standards at various concentrations. (B) Absorbance spectrum of purified and dissolved crystals from *F. iodinea* cerata (orange) diluted to produce a spectrum comparable to that of a mixture of 0.09 mM guanine and hypoxanthine standards. Using the curves from 0.09 mM guanine and hypoxanthine in a ratio of 81:19, a simulated spectrum was generated (dark blue) that closely matches that of the purified crystals. All samples were dissolved in methanol-HCl-water, 70:20:10 (v/v/v).

F. Confirmation by Thin Layer Chromatography

The purified *F. iodinea* crystals were analyzed by thin-layer chromatography as described in Methods, in parallel with pure guanine and hypoxanthine (Figure 13). The guanine and hypoxanthine standards were easily visualized with short wave UV light as spots of slightly different blue color with hypoxanthine appearing darker and traveling further than guanine, as previously reported (Rohrlich and Rubin, 1975). Two compounds

matching these mobilities and colors were most clearly visible for the crystals purified from the *F. iodinea* cerata and main body, thus identifying the major component of the crystals as guanine, and a minor component as hypoxanthine. These proportions are consistent with the spectroscopic analyses described above. The quantities of these compounds evident on the chromatogram were correspondingly lower for the sample from the main body, as the yield and final concentration of crystals from that tissue were considerably lower than from the cerata.

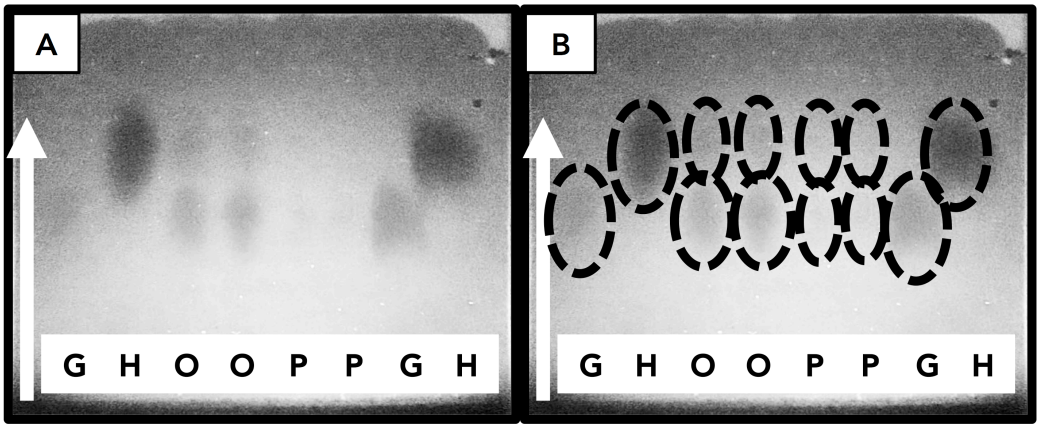

Figure 13. Thin layer chromatography confirms purine compositions of the reflective crystals. (A) TLC of purified and dissolved crystals from the orange cerata, O, and purple body, P, compared to pure guanine, G, and hypoxanthine, H, standards. Samples all were dissolved in 1 N HCl and developed with a methanol-HCl-water (70:20:10 v/v/v) solvent and visualized with short wave UV-light. (B). Same chromatogram as shown in (A), but with visible spots of UV absorption outlined for clarity.

These results suggest that the major component of the platelets is guanine, but that a significant amount hypoxanthine is also present in the structures. No other components were visible, indicating that no other nucleobases are significant components of the platelets.

IV. DISCUSSION AND CONCLUSIONS

The brilliant coloration of the nudibranch, *F. iodinea*, was found to be enhanced by multilayer reflectors composed of stacks of purine crystal platelets, each a doublet of tightly adhered crystalline layers. These reflective crystal stacks are similar in composition to those found in iridescent fish scales (Jordan et al., 2012; Gur et al., 2013), silver spiders (Mueller and Labhart, 2010; Levy-Lior et al., 2010), panther chameleons (Rohrlich and Rubin, 1975; Teyssier et al., 2015) and sapphirinid copepods (Gur et al., 2015), but unique in physical organization and optical effect. In contrast to the fixed positions or limited switching of orientation of the crystal stacks in these previously characterized systems, the reflectors of *F. iodinea* individually exhibit rotational and translational freedom. Consequently, as the reflectors tumble, they intermittently align with the incident light at the appropriate angle for maximum reflectance. This uniquely results in a dynamic, temporally varying, "sparkling" in the tissues.

These purine crystal reflectors, present in the cerata and body, are localized to a region of the endothelial monolayer near the basal lamina, as previously observed for reflective pigment granules in other aeolid species (Burgin, 1964; Martin and Walther, 2002; Martin et al., 2007), where they are concentrated in membrane bound compartments as well as free within the endothelial iridocytes. It is not yet determined, however, whether the free crystals are a characteristic of live cells or a result of tissue handling and processing. It is possible that the crystals are formed from amorphous guanine in these compartments in a process similar to that identified in silver spiders (Levy-Lior et al., 2010a; Weiner and Addadi, 2011) before their release. The reflectors tumble rapidly and stochastically in a manner independent of their confinement in the membrane bound compartments (Figure 4) and continued this movement when released into the surrounding medium, suggesting that

this phenomenon is not driven by cytoskeletal or other cellular mechanisms, but is governed by Brownian motion.

Table 1: Lattice parameters calculated from electron diffraction of *F. iodinea crystals*, simulated biogenic polymorphs and anhydrous guanine.

Source	Crystals Purified from Cerata, Experimental, Å	Crystals Purified from Body, Experimental Å	λ-Polymorph, Simulated[1], Å	Guanine Anhydrous[2], Experimental, Å	β-Polymorph, Simulated[1], Å
Lattice Dimension (a)	6.60 ± 0.03	6.54 ± 0.02)	6.38	3.55	3.59
Lattice Dimension (b)	13.64 ± 0.02	13.66 ± 0.05	9.73	9.69	9.72
Lattice Dimension (c)	18.77 ± 0.04	18.76 ± 0.02	18.39	16.35	18.34
Crystal Symmetry	Undetermined	Undetermined	Orthorhombic	Monoclinic	Monoclinic

[1]Parameters determined from *in silico* generated guanine polymorphs by Hirsch et al., 2015
[2]Parameters determined from experimental synchrotron data by Guille and Clegg, 2006.
Symmetry of the *F. iodinea* crystals cannot be decisively concluded from the ED data collected.

Electron diffraction of crystals isolated from the orange and purple tissue exhibit nearly identical lattice parameters of $a = 6.57 \pm 0.05$ Å, $b = 13.65 \pm 0.07$ Å and $c = 18.76 \pm 0.06$ Å. While UV-Vis spectroscopy and thin-layer chromatography strongly indicate that these crystals are composed primarily of guanine, with hypoxanthine as a minor component, these lattice parameters do not match those expected for chemically pure anhydrous guanine (Table 1). The crystal structure of anhydrous guanine is monoclinic, with space group $P2_1/c$ and cell dimensions a = 3.55, b = 9.69, c = 16.35 Å (Guille and Clegg, 2006). In this structure, the guanine molecules are linked together by N-H - - -N and N-H - - - O hydrogen bonds to form sheets, between which there are π-π stacking interactions. In the proposed structure, the lattice parameters *a* and *b* define the dimensions of the hydrogen bonding plane and, *c*, the dimension perpendicular to these planes (Guille and Clegg, 2006). The

predicted morphology of the anhydrous guanine crystals is prismatic, with elongation along the shortest crystallographic axis and perpendicular to the planar guanine molecules (Levy-Lior et al., 2008; Levy-Lior et al., 2010).

Biogenic guanine crystals from iridescent fish, silver spiders and sapphirinid copepods, however, do not exhibit this morphology (Levy-Lior et al., 2010; Gur et al., 2015; Hirsch et al., 2015). Instead, these crystals, like those discovered in *F. iodinea*, grow as thin plates with the shortest dimension in the direction that is expected to exhibit the highest growth rate. This results in crystal plates with the largest face parallel to the planar H-bonded network of guanine molecules (Levy-Lior et al., 2010a). In laboratory-grown, pure guanine crystals, the refractive index of this crystal face (determined to be the [102] face) is significantly higher (1.83) than that of one of the perpendicular faces (1.48) (Hinrichs et al., 2005; Levy-Lior et al., 2010). This pronounced birefringence has led to the proposition that organisms utilizing the photonic properties of guanine crystals have evolved a mechanism to inhibit the expected growth in the molecular stacking direction to optimize light reflectivity (Levy-Lior et al., 2008; Levy-Lior et al., 2010). Our data suggest that *F. iodinea* employs a similar mechanism to manipulate crystal morphology and lattice orientation.

Electron diffraction by the *F. iodinea* purine crystals in which the electron beam was oriented perpendicular to the largest crystal face display the same *mm* Laue symmetry as the 0*kl* diffraction patterns obtained from guanine crystals of a bright white Japanese koi (*Cyprinius carpio*) (Hirsch et al., 2015). This fish crystal ED pattern was shown to most closely match that simulated for an *in silico*- generated orthorhombic γ-polymorph of guanine (Hirsch et al., 2015). The lattice parameters calculated for this polymorph of a = 6.38 Å, b = 9.73 Å and c = 18.39 Å, where a and b define the dimensions of the hydrogen bonding plane and, c, the dimension perpendicular to these planes, are nearly identical to

those determined from the *F. iodinea* crystal diffraction patterns (see Table 1), with only the *b* parameter varying significantly. Considering that this alternative polymorph was generated assuming the crystals to be composed purely of guanine molecules, the variance in this dimension could be attributed to the incorporation of hypoxanthine into the crystal lattice, which would very likely strain and distort the lattice structure in the hydrogen bonding plane (Brice, 1975). It must further be noted that, while the ED patterns of purine crystals isolated from the white koi, and now *F. iodinea*, suggest an orthorhombic crystal habit, these data from the fish conflict with X-ray powder diffraction data from the same crystals, which suggest a monoclinic β-polymorph- a discrepancy discussed by Hirsch et al. (2015). This ambiguity renders the definitive assignment of a crystallographic space group to the *F. iodinea* crystals from only ED data impossible; it thus is not attempted here. For future work, X-ray powder diffraction patterns would provide the best additional structural information for further resolution of structure. Nevertheless, the ED data presented provide strong evidence that the reflective purine crystals of *F. iodinea* exhibit a morphology similar to the guanine crystals in the white koi.

Electron micrographs and ED patterns indicate that each individual crystal platelet from *F. iodinea* is actually composed of a doublet of closely adherent crystal layers (Figure 10; Figure 11). The random angle between ED patterns of the doublets within each platelet examined indicates that the two crystals are formed by independent nucleation rather than by twinning (Levy-Lior et al., 2010a). The close coupling and identical morphology of these crystal pairs suggest that they are grown within a single membrane-bound crystal chamber (Schmitter, 1971; Denton, 1970; Levy-Lior et al., 2010). The persistence of the doublets in nearly all of the *F. iodinea* crystal platelets isolated (following a procedure involving enzymatic digestion, vigorous mechanical mixing and centrifugation), suggests that these

doublets are not separated by a water-based or proteinaceous material. The doublets could, therefore, be joined by amorphous guanine, as proposed to be the case in analogous purine crystal doublets described from silver spiders (Levy-Lior et al., 2010a).

In the *in situ* sections (Figure 6; Figure 7), each platelet (composed of a crystal doublet) in a stack is separated from the next by unstained cellular material that, in other, systems, has simply been assumed to be cytoplasm (Levy-Lior et al., 2010a; Jordan et al., 2012; Jordan et al., 2014). The isolation of intact stacks from the tissue, following a physically rigorous purification procedure (Figure 10; Figure 11), suggests that this simplification does not hold in this system. Furthermore, the tumbling of full crystal stacks as a unit – a requirement for the proposed model of intermittent reflectance – would not be possible without the binding of the individual platelets to one another. This binding must be accomplished by a yet unidentified material, which cannot be assumed continuous with the surrounding cytoplasm.

The distribution and dimensions of the crystal stacks were found to be specific to different regions of the nudibranch. The stacks are much more abundant in the epidermal iridocytes of the cerata than in the body, as was evident both in the examination of tissues by light microscopy (Figure 3) and in the amount of crystalline material obtained from the tissues (Figure 12). Additionally, the crystals isolated from the cerata were larger and thicker, on average, than those isolated from the body (Figure 9; Figure 11). This difference in dimensions of crystals from these regions suggests a physical basis for the observed variation in the color of light they reflect. Basic optical theory posits that the optical path length of a layer in a quarter wave stack governs the peak wavelength of reflectance of the stack. In other words, a quarter wave stack of thinner layers will reflect shorter wavelengths compared to a quarter wave stack of thicker layers, which will reflect a longer wavelength

(e.g., Joannopoulus et al., 2011). Consequently, assuming the *F. iodinea* crystal stacks function as quarter wave stacks, the thicker crystals of the cerata are expected to reflect light of longer wavelengths than the thinner crystals of the body. Moreover, a reflector with little variation in the layer thickness throughout the structure produces a narrowband "colored" reflectivity; and, conversely, a structure composed of layers with a distribution of thicknesses produces a broadband "silver" reflectivity (Jordan et al., 2014). The significant variation in the thickness of the crystals from the cerata, therefore, agrees with the observed silver reflectance, while the more uniform thickness of the crystals from the body agrees with their observed blue reflectance. Thus, *F. iodinea* provides an example of how, within a single animal, the control over the distribution of layer thicknesses in the reflector enables production of narrowband "colored" reflectivity and broadband "silver" reflectivity (Figure 14) (Jordan et al., 2014).

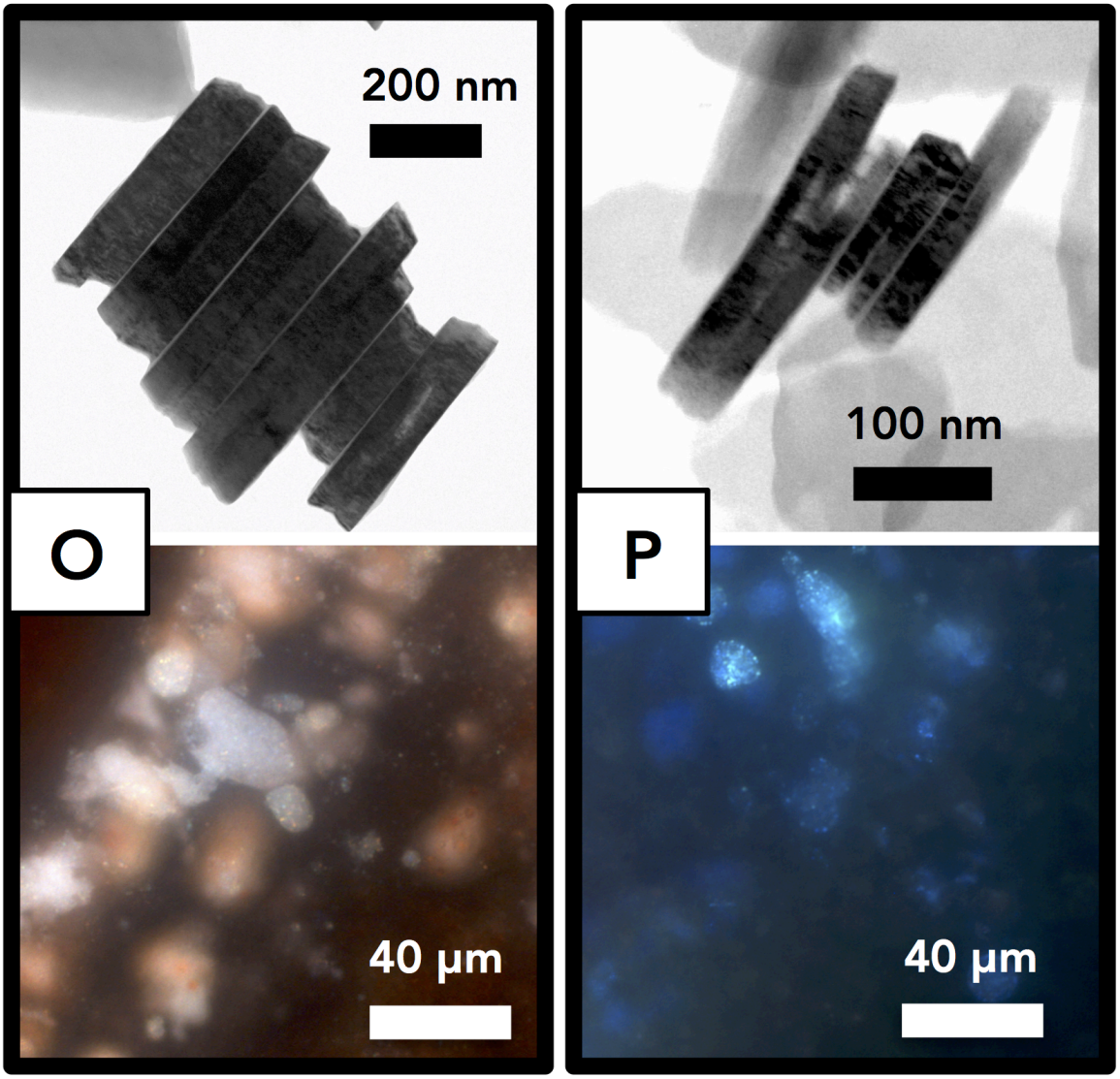

Figure 14. Comparison of the broadband silver reflectance produced by the thicker, more disordered platelets in the orange cerata (O) and the narrowband blue reflectance produced by the thinner, more regular platelets in the purple body (P).

The epidermal iridocytes of *F. iodinea* are capable of manipulating crystal growth in a tissue-specific manner, producing purine crystal stacks apparently comparable in composition but differing in dimension and abundance in different regions of the body. The resulting differences in reflective crystals with unique optical properties in different regions of the animal parallels the differences in astaxanthin pigmentation, such that the brilliant orange cerata are highly reflective, while the purple body is significantly less so. This color

pattern has been proposed both to advertise toxicity as a means of reducing predation, and to attract predators to the stinging nematocysts concentrated in the peripheral cerata and away from the viscera of the body (Thompson, 1960a; Edmunds, 1966; Mappes, 2005). One conjecture is that these reflective regions contribute to this contrast, effectively turning the cerata into reflective optical lures (Doucet, 2009; Su, 2015).

IV. LITERATURE CITED

Aguado, F. and Marin, A. 2007. Warning coloration associated with nematocyst-based defences in aeolidiodean nudibranchs. *J. Mollus. Stud.***73,** 23–28.

Brice, J. C. 1975. Some thermodynamic aspects of the growth of strained crystals. *Journal of Crystal Growth***28,** 249–253.

Burgin, U. 1964. The Color Pattern of *Hermissinda crassicornis* (Eschscholtz 1831). *The Veliger***7,** 205–215.

Crookes, W. J. *et al.* 2004. Reflectins: the unusual proteins of squid reflective tissues. *Science***303,** 235–238.

Doucet, S. M. and Meadows, M. G. 2009. Iridescence: a functional perspective. *Journal of The Royal Society Interface***6,** S115–S132.

Dougherty, L. F., Johnsen S., Caldwell, R. L. and Marshall, N. J. 2014. A dynamic broadband reflector built from microscopic silica spheres in the 'disco' clam *Ctenoides ales*. *Journal of The Royal Society Interface***11,** 20140407.

Denton, E. J. 1970. Review Lecture: On the Organization of Reflecting Surfaces in Some Marine Animals. *Philosophical Transactions of the Royal Society of London B: Biological Sciences***258,** 285–313.

Edmunds, M. 1966. Protective mechanisms in the Eolidacea (Mollusca Nudibranchia). *Journal of the Linnean Society of London, Zoology***46,** 27–71.

Fox, D. L. 1976. Animal Biochromes and Structural Colours: Physical, Chemical, Distributional & Physiological Features of Coloured Bodies in the Animal World. *University of California Press*.

Fleming, P. A., Muller D. and Bateman, P. W. 2007. Leave it all behind: a taxonomic perspective of autotomy in invertebrates. *Biol. Rev.***82,** 481–510.

Goodheart, J. A., Bazinet, A. L., Collins, A. G. and Cummings, M. P. 2015. Relationships within Cladobranchia (Gastropoda: Nudibranchia) based on RNA-Seq data: an initial investigation. *Open Science***2,** 150-196.

Greenwood, P. and Mariscal, R. 1984. Immature Nematocyst Incorporation by the Aeolid Nudibranch *Spurilla-Neapolitana*. *Mar. Biol.***80,** 35–38.

Guille, K. and Clegg, W. 2006. Anhydrous guanine: a synchrotron study. *Acta Cryst. C*.**62,** 515–517.

Gur, D. *et al.* 2015. Structural Basis for the Brilliant Colors of the Sapphirinid Copepods. *J. Am. Chem. Soc.***137,** 8408–8411.

Herring, P. J. 1994. Reflective systems in aquatic animals. *Comparative Biochemistry and Physiology Part A: Physiology***109,** 513–546.

Joannopoulus, J., Meade, R., Johnson, S. and ,Winn J. 2011. Photonic Crystals. *Princeton University Press*.

Hinrichs, K., Silaghi, S. D., Cobet, C., Esser, N. and Zahn, D. R. T. 2005. Ellipsometry from infrared to vacuum ultraviolet: Structural properties of thin anisotropic guanine films on silicon. *Phys. Stat. Sol.(b)***242,** 2681–2687.

Hirsch, A. *et al.* 2015. 'Guanigma': The Revised Structure of Biogenic Anhydrous Guanine. *Chemistry of Materials***27,** 8289–8297.

Jordan, T. M., Partridge, J. C. and Roberts, N. W. 2012. Non-polarizing broadband multilayer reflectors in fish. *Nat. Photonics***6,** 759–763.

Jordan, T. M., Partridge, J. C. and Roberts, N. W. 2014. Disordered animal multilayer reflectors and the localization of light. *J. R. Soc. Interface***11**.

Kester, D. R., Duedall, I. W., Connors, D. N. and Pytkowicz, R. M. 1967. Preparation of artificial seawater. *Limnology and oceanography***12,** 176–179.

Land, M. F. 1972. The physics and biology of animal reflectors. *Progress in Biophysics and Molecular Biology***24,** 75–106.

Levy-Lior, A. *et al.* 2008. Biogenic guanine crystals from the skin of fish may be designed to enhance light reflectance. *Cryst. Growth Des.***8,** 507–511.

Levy-Lior, A. *et al.* 2010. Guanine-Based Biogenic Photonic-Crystal Arrays in Fish and Spiders. *Adv. Funct. Mater.***20,** 320–329.

Mappes, J., Marples, N. and Endler, J. A. 2005. The complex business of survival by aposematism. *Trends in Ecology & Evolution***20,** 598–603.

Martin, R. *et al.* 2007. Granular chitin in the epidermis of nudibranch molluscs. *Biol. Bull.***213,** 307–315.

Martin, R. 2003. Management of nematocysts in the alimentary tract and in cnidosacs of the aeolid nudibranch gastropod *Cratena peregrina*. *Mar. Biol.* **143,** 533–541.

Martin, R. and Walther, P. 2003. Protective mechanisms against the action of nematocysts in the epidermis of *Cratena peregrina* and *Flabellina affinis* (Gastropoda, Nudibranchia). *Zoomorphology***122,** 25–32.

McBeth, J. W. 1972. Carotenoids from nudibranchs. *Comparative Biochemistry and Physiology Part B: Comparative Biochemistry***41,** 55–68.

Miller, J. A. and Byrne, M. 2000. Ceratal Autotomy and Regeneration in the Aeolid Nudibranch *Phidiana crassicornis* and the Role of Predators. *Invertebrate Biology***119,** 167–176.

Mueller K. P. and Labhart T. 2010. Polarizing optics in a spider eye. *J. Comp. Physiol. A -Neuroethol. Sens. Neural Behav. Physiol.***196,** 335–348.

Schmitter, R. E. 1971. The Fine Structure of *Gonyaulax Polyedra*, a Bioluminescent Marine Dinoflagellate. *Journal of Cell Science***9,** 147–173.

Schneider, C. A., Rasband, W. S., Eliceiri. K. W. *et al.* 2012. NIH Image to ImageJ: 25 years of image analysis. *Nat methods***9,** 671–675.

Seago, A. E., Brady, P., Vigneron, J.-P. and Schultz, T. D. 2009. Gold bugs and beyond: a review of iridescence and structural colour mechanisms in beetles (Coleoptera). *Journal of The Royal Society Interface* **6,** S165–S184.

Striedter, G. F., Avise, J.C., Ayala, F.J. 2013. *In the Light of Evolution: Volume VI: Brain and Behavior.* National Academies Press.

Su, S., Lim, M. and Kunte, K. 2015. Prey from the eyes of predators: Color discriminability of aposematic and mimetic butterflies from an avian visual perspective. *Evolution***69,** 2985–2994.

Teyssier, J., Saenko, S. V., van der Marel, D. and Milinkovitch, M. C. 2015. Photonic crystals cause active colour change in chameleons. *Nat Commun***6,** 6368.

Thompson, T. 1960a. Defensive Adaptations in Opisthobranchs. *J. Mar. Biol. Assoc. U.K.***39,** 123–134.

Thompson, T. 1960b. Defensive Acid-Secretion in Marine Gastropods. *J. Mar. Biol. Assoc. U.K.***39,** 115–122.

Vukusic, P. and Sambles, J. R. 2003. Photonic structures in biology. *Nature***424,** 852–855.

Wägele, H. 2004. Potential key characters in Opisthobranchia (Gastropoda, Mollusca) enhancing adaptive radiation. *Organisms Diversity & Evolution***4,** 175–188.

Weiner S. and Addadi L. 2011. *Crystallization Pathways in Biomineralization.* Annual Review of Materials Research**41,** 21–40.

Zhao, S. *et al.* 2015. Broadband and polarization reflectors in the lookdown, *Selene vomer*. *Journal of The Royal Society Interface***12,** 20141390.